Bathymetric influences on Antarctic ice-shelf melt rates

D. N. Goldberg[1], T. A. Smith[2], S. H. K. Narayanan[3], P. Heimbach[2,4,5], M. Morlighem[6]

[1]School of Geosciences, University of Edinburgh, Edinburgh, United Kingdom
[2]Oden Institute for Computational Engineering and Sciences, The University of Texas at Austin, Austin, Texas
[3]Mathematics and Computer Science Division, Argonne National Laboratory
[4]Jackson School of Geosciences, The University of Texas at Austin, Austin, Texas
[5]Institute for Geophysics, The University of Texas at Austin, Austin, Texas
[6]University of California Irvine, Department of Earth System Science, Irvine, California

Key Points:

- Sensitivity of ocean-driven ice-shelf melt is investigated using the adjoint of an ocean model
- Sensitivity of ice-shelf melt to ocean bathymetry is concentrated on isolated bathymetric features, with wide areas exerting little control
- Results could be used to prioritize locations of high-fidelity investigations of sub-ice shelf cavity geometry

Abstract

Ocean bathymetry exerts a strong control on ice sheet-ocean interactions within Antarctic ice-shelf cavities, where it can limit the access of warm, dense water at depth to the underside of floating ice shelves. However, ocean bathymetry is challenging to measure within or close to ice-shelf cavities. It remains unclear how uncertainty in existing bathymetry datasets affect simulated sub-ice shelf melt rates. Here we infer linear sensitivities of ice shelf melt rates to bathymetric shape with grid-scale detail by means of the adjoint of an ocean general circulation model. Both idealised and realistic-geometry experiments of sub-ice shelf cavities in West Antarctica reveal that bathymetry has a strong impact on melt in localised regions such as topographic obstacles to flow. Moreover, response of melt to bathymetric perturbation is found to be non-monotonic, with deepening leading to either increased or decreased melt depending on location. Our computational approach provides a comprehensive way of identifying regions where refined knowledge of bathymetry is most impactful, and also where bathymetric errors have relatively little effect on modelled ice sheet-ocean interactions.

1 Introduction

The bathymetry of the ocean exerts a leading order influence on ocean circulation, both at global and regional scales (e.g., Roberts & Wood, 1997; D. Marshall, 1995; Hughes & Killworth, 1995; Gille et al., 2004). It plays a key role in regulating exchanges between the Antarctic continental shelf and the deep ocean (e.g., Walker et al., 2013; Thoma et al., 2008; Graham et al., 2016; Thompson et al., 2018) and in setting circulation patterns on the continental shelf (e.g., Padman et al., 2010; Jacobs et al., 2011; Arneborg et al., 2012; Cochran & Bell, 2012; De Rydt et al., 2014; Rosier et al., 2018; Wählin et al., 2020). Its role in ice sheet-ocean interactions is accentuated by the fact that a large part of the Antarctic ice sheet rests well below sea level (Bentley et al., 1960), with a sizable portion of its margins terminating in large floating ice shelves. These ice shelves slow the speed of fast-flowing ice streams through buttressing (Thomas & Bentley, 1978; Thomas, 1979). Therefore the collapse or retreat, melting and associated thinning of ice shelves, while having a limited direct effect on sea level (Jenkins & Holland, 2007), can result in increased grounded ice loss from the continent (Shepherd et al., 2004) – a loss which may be amplified due to a positive feedback involving the geometry of sub-ice sheet topography known as the Marine Ice Sheet Instability (Schoof, 2007; Joughin et al., 2014).

The circulation of water under ice shelves is of great importance in the Amundsen and Bellingshausen Seas, West Antarctica, where intrusions of warm, salty Circumpolar Deep Water (CDW) from the Antarctic Circumpolar Current occur (Jacobs et al., 1996; Jenkins et al., 1997; Thoma et al., 2008; Arneborg et al., 2012; Jenkins et al., 2016; Zhang et al., 2016), promoted in part by continental shelf geometry in these regions (Pritchard et al., 2012). Regional atmospheric forcing and sea-ice states lead to stable stratification of the water column that limits mixing of this dense water with cool surface layers (Petty et al., 2013), allowing higher rates of ice-shelf mass loss than elsewhere in Antarctica (Jenkins, 2016). CDW-driven ice-shelf melt is not strictly limited to the Amundsen and Bellingshausen Seas (Gwyther et al., 2014; Greene et al., 2017), and climate modelling suggests it could become more widespread around Antarctica under climate change scenarios (Hellmer et al., 2012). The ability of this warm, dense water to drive ice-shelf melt depends to a large extent on how it is steered or blocked by bathymetry on the continental shelf and within the cavity.

Despite considerable efforts devoted to improving Antarctic-wide estimates of bed topography (see most recently Morlighem et al. (2020)), our knowledge of bathymetry in large parts of the marine margins of the ice sheet is highly uncertain. Direct observations of the ocean seafloor near Antarctica are beset by difficulties such as remoteness and sea ice cover (Nitsche et al., 2007). Collecting bathymetric data under floating ice shelves is even less practical. Autonomous submersibles capable of measurements under floating ice shelves are only beginning to be deployed. With a $\sim$300 m swath, extensive coverage of under-ice shelf bathymetry is not feasible (e.g., Jenkins et al., 2010). Airborne gravity sensing offers an alternative means of bathymetric measurement (e.g., Tinto & Bell, 2011; Millan et al., 2017); however, gravimetric inversions are subject to errors related to resolution and geologic uncertainty. Seismic observations of the bed do not rely on lithology assumptions, but as they are generally ground-based, data-gathering is expensive and often limited to point estimates (e.g., Rosier et al., 2018).

Previous studies have addressed this uncertainty in the context of a physical ocean model by considering idealised bathymetries (De Rydt et al., 2014; Zhao et al., 2018) or testing different bathymetry products (Schodlok et al., 2012; Goldberg et al., 2019). To date, no modelling study has investigated the melt response to the full range of uncertainty in sub-ice shelf bathymetry. Here, we aim to provide a better understanding of

this uncertainty by estimating the sensitivity of ocean-driven ice-shelf melt rates to bathymetry in a West Antarctic sector.

Previously, Losch & Heimbach (2007) developed a method to calculate the sensitivity of circulation metrics (e.g., the strength of meridional overturning or zonal mass transport) to ocean bathymetry using the adjoint of the Massachusetts Institute of Technology general circulation model (MITgcm). In general, adjoint models generate linearized sensitivities of model outputs to an arbitrarily large set of input parameters (Wunsch, 1996), providing a computationally efficient means for investigating the impacts of grid-scale uncertainties. To avoid tedious "by-hand" differentiation of a complex ocean general circulation model, Losch & Heimbach (2007) made use of *algorithmic differentiation* (AD) software, which has been used extensively with the MITgcm (Heimbach et al., 2005; Wunsch et al., 2009). However, this adjoint model involving bathymetry sensitivities has not been extensively used since, and has not previously been applied to sub-ice shelf circulation.

In this paper, we "revive" the adjoint model infrastructure for treating bathymetry as an uncertain input variable, and employ this framework to investigate the impacts of bathymetric uncertainty on ice-shelf melt rates. Two important technical improvements are (i) the use of an open-source AD tool to generate the adjoint model, and (ii) improved treatment of the implicit free-surface solver in generating the adjoint model. These are summarized in Section 2, where we briefly discuss our methodology, including our adjoint approach and our updates to the MITgcm code base (with further details in the Section 1 of the supplementary material). We apply our framework to an idealised domain and analyse the resulting sensitivities (Section 3). We then carry out a study of the Crosson and Dotson ice shelves in the Amundsen Sea Embayment (Section 4), and conclude with discussion in Section 5.

2 Methodology

2.1 Modelling of ice-ocean interactions

We simulate sub-ice shelf circulation with the MITgcm, an open-source general purpose finite-volume code which solves the hydrostatic primitive equations on the rotating sphere governing ocean flow (J. Marshall et al., 1997). (The code has nonhydrostatic capability but it is not used in this study.) Since its inception, code "packages" repre-

senting modularized parameterizations, numerical algorithms, and separate climate components have been introduced. One such package, `SHELFICE` (Losch, 2008), allows for circulation in cavities beneath ice shelves that may be many hundreds of meters deep. `SHELFICE` also calculates melt rates and the associated heat and salt fluxes at the ice-ocean interface based on under-ice ocean properties using a viscous sublayer parameterization (Holland & Jenkins, 1999). In this study we use the velocity-dependent form of the melt parameterization (Dansereau et al., 2014), unless otherwise stated. The ice-ocean model has successfully run the Ice Shelf Ocean Model Intercomparison Experiment (ISOMIP; Holland et al. (2003)), the experimental setup of which forms the basis for our first experiment.

2.2 Discretization of bathymetry in the MITgcm

The vertical discretization of bathymetry in MITgcm is distinct from other aspects of discretization in the model, and given the nature of this study it deserves mention. To allow for varying bathymetry but avoid dramatic steps due to the prescribed vertical level thicknesses, a *partial cell* discretization is implemented (Adcroft et al., 1997), where bottom cells can be partially fluid-filled with fraction h_f, down to a minimum specified thickness $h_{f,min}$. This means that vertical cell faces (i.e. faces normal to horizontal directions) are partially fluid-filled as well, which is important as cell faces determine volume and tracer transport. Due to memory requirements, bathymetry is represented as piecewise-constant (as opposed to piecewise-linear), meaning fluid fractions at cell faces are a function of depth at adjacent cell centers (see Fig. 1(a)). This choice has implications for algorithmic differentiation of bottom sensitivity, as discussed below.

2.3 Adjoint model

An ocean model may be conceptualised as a mathematical function that maps an input vector $\mathbf{x}_{in}$ onto an output vector $\mathbf{x}_{out}$. The input vector $\mathbf{x}_{in}$ consists of the discretized initial conditions for the oceanic state, as well as all inputs required to integrate the partial differential equations that govern the circulation of the ocean, including discretized input fields for surface (forcing) and bottom (bathymetry) boundary conditions. $\mathbf{x}_{out}$ consists of all prognostic model output (generally of a much higher dimension than that of $\mathbf{x}_{in}$), or diagnostic functions thereof, including scalar-valued metrics. It is often of interest to know how perturbations in $\mathbf{x}_{in}$ affect $\mathbf{x}_{out}$, or how they affect quantities

that depend on $\mathbf{x}_{out}$ (sometimes referred to as "objective functions" or "quantities of interest"). An example application of an adjoint model might be investigating how Atlantic meridional overturning is sensitive to global patterns of precipitation (Pillar et al., 2016; Smith & Heimbach, 2019).

The *sensitivity vector*, i.e. the gradient of the quantity of interest with respect to $\mathbf{x}_{in}$, could be determined by perturbing separately each element of $\mathbf{x}_{in}$ and observing the model response (formally, inferring a directional derivative); however, such an approach for computationally intensive models and input vectors of high dimension is impractical. However, forming the *adjoint* of the model (or, more precisely, the adjoint of its Jacobian) provides an alternative means (Errico, 1997), enabling calculation of the sensitivity vector at a computational cost that does not depend on the dimension of $\mathbf{x}_{in}$.

Differentiation of the ocean model can be carried out at the equation level (Sirkes & Tziperman, 1997), though this approach requires a separate code that must be updated when the ocean model is modified. Another method – and the one used in this work – is Algorithmic Differentiation (AD), which uses a software tool to automate differentiation of the model at the discrete (code) level. In this study, two different AD tools are used: *Transformations of Algorithms in Fortran* (TAF; Giering et al. (2005)) and OpenAD (Utke et al., 2008). Both are source-to-source tools, meaning code is generated in the native language (as opposed to operator-overloading). Both tools have been used to generate the MITgcm adjoint; TAF, a commercial product, has been used more extensively with the MITgcm, while OpenAD is a more recent open-source tool.

While AD presents great benefits in differentiating complex numerical codes and keeping the adjoint code in synchronization with the parent numerical code, some degree of manual intervention is generally required. In the present study changes to the adjoint generation were necessary to facilitate efficient computation, the foremost dealing with the way in which MITgcm evolves the ocean free surface. These and other details are discussed in detail in Section 1 of the supplementary material (Giles et al., 2002).

3 Idealised Experiment

To gain insight into how bathymetry modulates the interaction between ocean circulation and ice shelf melt, we first examine sensitivity of melt to bathymetry in an idealized domain, which is a slightly modified version of the computational domain used in

the Ice Shelf Ocean Model Intercomparison Project (ISOMIP; Holland et al. (2003)). In the MITgcm implementation of the standard ISOMIP setup, the ocean circulates within a closed rectangular domain with a flat bathymetry of 900 m depth, with an initially uniform temperature of -1.9°C. A zonally-uniform ice-shelf draft slopes meridionally from 700 m depth to 200 m depth over about 450 km, and is constant north of this point. We use a resolution of 30 m in the vertical, 0.3° zonally, and 0.1° meridionally (amounting to ∼8.5 km zonally and ∼11 km meridionally. A full description can be found in Losch (2008); to enable a direct comparison with that study, we specify velocity-independent turbulent exchange coefficients in the melt rate parameterisation. We modify the ISOMIP domain by introducing a zonally-constant ridge in the bathymetry just south of the point of deepening of the ice shelf. The meridional expression is a half-cosine "bump" with a width of 2° latitude and a height of 200 m above the uniform seafloor (Fig. 2(a)), and we refer to our experiment as "ISOMIP-bump". This bathymetry is inspired by bathymetric ridges identified under a number of Antarctic ice shelves (e.g., Jenkins et al., 2010; Wei et al., 2019), which are found to strongly control the transport of relatively warm water within ice shelf cavities (De Rydt et al., 2014; Dutrieux et al., 2014).

Our adjoint experiment is as follows: the ISOMIP-bump model is run forward in time for 2 model years, and the spatial integral of the melt rate in the final time step is evaluated as our quantity of interest J:

$$J = \sum_i d_i m_i, \tag{1}$$

where d_i and m_i are the area of, and melt rate within, horizontal cell i. The adjoint model accumulates sensitivity of J with respect to bathymetry back in time along the 2-year simulation trajectory and thus depends on the state of the entire 2-year run, not just the final state. Thus, to mitigate impacts of equilibration, we begin the model run from a "spun-up" state rather than a quiescent one. The model is thus first spun-up for 3 years, and the resulting state forms the initial conditions for our 2-year forward and adjoint run.

3.1 Results

The melt (and accretion) rate at the final time in the adjoint experiment (Fig. 2(b)) has a similar pattern to that of Mathiot et al. (2017) (their Fig. 2), although melt and accretion rates are generally smaller (with the peak accretion being about 1/3 of that

of Mathiot et al. (2017)), and there is a "tongue" of melt rates bisecting the accretion region over the ridge. The barotopic circulation also differs slightly with respect to the standard ISOMIP experiment: rather than a broad cyclonic gyre, there is a narrow anticyclonic anomaly on the north side of the ridge (Fig. 2(b)). Barotropic flow is primarily along the ridge, crossing it primarily near the eastern and western boundaries, similar to what has been shown in a simplified two layer model (Zhao et al., 2018). Zonally-averaged temperatures (Fig. 2(a)) suggest slightly cooler waters at depth just south of the ridge as opposed to the northern flank. The smaller melt and accretion rates as compared to Mathiot et al. (2017) could reflect the fact that our simulation has not yet reached steady-state – indicating that the presence of the ridge increases the time to reach a new steady-state. Alternatively, the ridge may act as a potential vorticity barrier, preventing warmer bottom waters from coming in contact with the shelf (De Rydt et al., 2014; Zhao et al., 2018).

The adjoint-derived sensitivities are shown in Fig. 3(a). In this figure, shading indicates $\frac{\partial J}{\partial \delta R_i}$, where R_i is bottom depth at location i. Positive values indicate locations where raising the seafloor will increase integrated melt, and negative values indicate where lowering the seafloor will increase melt. There are distinct broad-scale patterns in the sensitivities, particularly over the ridge itself. Across much of the zonal extent of the ridge there is negative sensitivity (region 1 in Fig. 3(a)), indicating a lowering of the ridge would increase melt. Near the eastern boundary, however, there is a region with strongly positive sensitivities (region 2). Northward of the ridge where both bathymetry and ice draft are constant, there is a broad dipole pattern, with positive sensitivities toward the center (region 3) and negative toward the east (region 4). In our investigation below we focus on these four regions, foregoing close analysis of areas with negligible influence on melt (such as southward of the ridge), and areas where there is strong spatial variability in the sensitivity, such as the western edge of the ridge.

In order to ensure that adjoint sensitivity patterns did not arise from issues involving Algorithmic Differentiation, both AD tools (OpenAD and TAF) were used to generate sensitivities. (A similar approach was taken in in Heimbach et al. (2011).) The differences in the sensitivities, likely arising from numerical truncation, were negligible, and are not shown.

3.2 Finite-amplitude perturbations of bathymetry

As with any adjoint-based study, it is important to verify the adjoint-derived sensitivities by perturbing the input, or *control*, field in the forward model, i.e. by estimating finite-difference approximations to the gradients that the adjoint model calculates. In the MITgcm this type of "gradient check" is more challenging when dealing with model bathymetry than with other control variables, as demonstrated in Fig. 1(b): finite perturbations of bathymetry can change grid structure, for example by adding new cells to, or removing cells from, the domain. Neither operation is differentiable, and hence linearized sensitivities may not reflect model responses to perturbed bathymetry. Additionally, bathymetric perturbations may not be as anticipated, as thicknesses of cells will be adjusted by the model initialization to ensure no partial cell is thinner than $h_{f,min}$.

These challenges aside, we implement finite perturbations to bathymetry in order to test the results from the adjoint model, but our experiment design is intended to minimize the above complications. Rather than perturb values in individual cells, we apply perturbation *patterns*. We carry out experiments with four separate perturbation patterns, naturally selected in regions of high sensitivity, where bathymetric perturbations exhibit the greatest control on melt-rates, as shown in Fig. 3(a). The patterns have a Gaussian profile:

$$\delta R(\phi,\lambda) = \delta R_0 \exp\left(-\frac{(\phi-\phi_0)^2}{L_\phi^2} - \frac{(\lambda-\lambda_0)^2}{L_\lambda^2}\right) \tag{2}$$

where ϕ and λ are latitude and longitude. ϕ_0, λ_0, L_ϕ and L_λ vary with experiment but the location and radii of the perturbations can be seen from Fig. 4 for each region. Different values of δR_0 are considered as described below.

For a given depth perturbation δR, the linear response to J predicted by the adjoint is

$$\delta J = \sum_i \delta J_i = \sum_i (\delta R_i)(\delta^* R_i), \tag{3}$$

where δR_i is the finite perturbation to bathymetry in ocean column i and $\delta^* R_i = \frac{\partial J}{\partial R_i}$ is the bathymetric sensitivity in i as calculated by the adjoint. If the adjoint model is accurate, Eqn. (3) should be fairly accurate for small values of δR_i. This is the case for $\delta R_0 = 0.1$ m (Fig. 3(b)). Positive and negative perturbations are considered in regions 1 and 2; in regions 3 and 4 only positive perturbations are examined as negative perturbations would lower bathymetry beyond the extent of the computational grid. For larger perturbations ($\delta R_0 = 10$ m), linear sensitivities give fairly accurate predictions in re-

gions 2, 3 and 4; in region 1 (the center of the ridge), the linear approximation underestimates the response. Closer inspection reveals that, when bathymetry is perturbed in the center of the ridge, a number of fluid-containing cells become empty. Similarly, when regions 1 and 2 are negatively perturbed with $\delta R_0 = 10$ m, an even larger number of previously empty cells become fluid-filled. These non-differentiable changes could explain the underestimates.

Examining the perturbed melt rates and circulation provides further insight into the sensitivity patterns produced by the adjoint model. Bathymetric rises in regions 3 and 4 affect melt rates predominantly to the north (i.e. oceanward) of the bathymetric ridge (Fig. 4(c,d)). Examination of the perturbed barotropic circulation (Fig. S2(c,d) of the supplementary material) shows that in both cases, an anticyclonic region develops to the west of the rise, and a cyclonic region to the east. The pattern is reminiscent of the interaction between a jet and a topographic rise (Huppert & Bryan, 1976; Holland et al., 2003), with the broad cyclonic cell in this region (Fig. 2(b)) generating the background flow. As this cell transports water away from the cold outflow from the cavity before it circulates back toward the ridge, it is likely that perturbations which strengthen/oppose this circulation will increase/decrease melt – although as Figs. 4(c,d) indicate, this effect does not penetrate beyond the ridge.

For perturbations to the ridge itself (regions 1 and 2), there is a more complex melt response, the effects of which are felt more strongly to the south of the ridge (Fig. 4(a,b)). In terms of the circulation, there is a similar response to the barotropic stream function as with regions 3 and 4, although complicated by the varying background topography. In the case of a raised bump on the eastern ridge (region 2), the leading effect on the circulation is a southward shift of the warm jet travelling eastward along the ridge (Supplemental Fig. S2(b)). There is decreased melt in the southeast of the ice shelf, but this is offset by stronger melt above the ridge and decreased accretion in the western outflow (Fig. 4(b)). A rise in the center of the ridge has the opposite effect, decreasing melt over the ridge 4(a)).

While these results are highly idealized, they are nonetheless instructive regarding bathymetric influence on melt in ice-shelf cavities with topographic obstacles: (1) bathymetry in areas "protected" by the obstacle play a relatively small role in controlling melt; (2) the height of the obstacle has a strong influence on melt, but the direc-

tion, or sign, of the influence may depend on the location along the ridge and related to the background flow that is set up by the geometry; and (3) bathymetry oceanward of the obstacle can influence melt as well, by controlling the circulation that brings warm water toward the ice-shelf cavity. These insights inform the interpretation of sensitivities in simulations with realistic bathymetry.

The perturbation experiments offer a further lesson: an adjoint indicates linear sensitivities of a scalar objective function, such as integrated melt rates – but it does not indicate how the *pattern* of melt will change in response to inputs. If melt in a certain location, or changes of a specific pattern, are of interest, a different objective function should be considered.

4 Realistic experiment: Dotson and Crosson ice shelves

The Dotson and Crosson Ice Shelves are relatively small but strongly thermally-forced ice shelves in the Amundsen Sea Embayment of West Antarctica (Fig. 5(a)). Recently, these ice shelves, as well as the ice streams that flow into them, have been the subject of focused glaciological and oceanographic study (e.g., Randall-Goodwin et al., 2015; Goldberg et al., 2015; Miles et al., 2016; Gourmelen et al., 2017; Jenkins et al., 2018; Lilien et al., 2018). Moreover, ice-ocean interactions under these ice shelves have significance for biological productivity in the Southern Ocean: levels of carbon sequestration in the highly productive Amundsen Polynya are thought to be connected strongly to ice-shelf melt volume (Gerringa et al., 2012; Yager et al., 2012). A recent modelling study by Goldberg et al. (2019) showed that the choice of bathymetric product has a significant influence on the melt rates modelled for these ice shelves. Therefore, it is an ideal region in which to examine the sensitivity of melt to bathymetry.

4.1 Model configuration

Our ocean model configuration is based on that of Goldberg et al. (2019). We use the MITgcm with the `SHELFICE` package and with ice-shelf draft and bathymetry based on Millan et al. (2017). At ocean-facing boundaries we impose conditions on temperature, salinity and velocity from a regional simulation by Kimura et al. (2017). However, there are important differences with the configuration of Goldberg et al. (2019), which are largely influenced by practical considerations concerning the performance of the OpenAD-

generated adjoint. Adjoint models generally require more computing time than the forward models from which they derive, requiring in some cases recomputation to avoid intractable memory requirements (Griewank & Walther, 2008). The 4-year simulations conducted by Goldberg et al. (2019) ran for approximately 32 hours on 48 cores on the Research Councils UK (RCUK) ARCHER supercomputer (discounting queueing times in between batches), meaning an adjoint experiment might require up to several weeks' wall-clock execution time leading to large delays in our investigations and potentially irresponsible energy usage. (This scaling is based on the timings of experiments in this study and not a rigorous analysis of OpenAD performance.) Thus, modifications were made to reduce computational expense and facilitate adjoint computation.

A 2-km grid was used as opposed to a 1-km grid, and the time step increased from 150 to 300 seconds. Additionally, a larger horizontal eddy viscosity, $\nu_H = 120$ m^{2}s^{-1}, was imposed, for the following reason. The ocean adjoint model is a distinct numerical code – related to the forward ocean model but with its own stability constraints, arising in part from the chosen quantity of interest, which informs the boundary and initial conditions of the adjoint model. It is often the case that the adjoint of a nonlinear forward model produces sensitivity patterns with sharp spatial gradients, which grow in amplitude over time because the model lacks the nonlinear feedbacks to damp them, resulting in numerical instabilities. Hoteit et al. (2005) showed that a stabilization of the adjoint may be achieved with a larger value of ν_h for the adjoint model, while retaining a smaller eddy viscosity in the forward model, but such a capability for the OpenAD-MITgcm adjoint is not yet available. We point out that our chosen value for ν_h is smaller than that used in the ice-ocean interaction study of Dansereau et al. (2014), which also used the `SHELFICE` package of MITgcm.

Additionally the open boundary conditions of our computational domain, which represent interactions with the Antarctic Circumpolar Current (i.e. the ocean-facing boundary conditions), were made time-constant rather than time-varying as in Goldberg et al. (2019). As discussed in Section 4.3, this better enables the assessment of the timescale of adjustment to boundary conditions. Velocity, temperature and salt conditions from Kimura et al. (2017) were averaged over 2011 (the highest-melt year in the the Goldberg et al. (2019) study), allowing for a shorter experiment.

Finally, the Millan et al. (2017) bathymetry was adjusted over a region of approximately 90 km^2 close to the junction between Crosson and Dotson Ice Shelves, where the Kohler range extends into the ice-shelf cavity (Fig. 5(a)). In this area, the Millan bathymetry suggests a significant ridge with a peak less than 300 m below sea level. Without modification, this ridge would lead to very thin ocean columns in our model, effectively limiting ocean transport to the narrow region between the ridge and Bear Peninsula. However, observed melt rate patterns (Gourmelen et al., 2017; Goldberg et al., 2019) show high melt rates in this location, suggesting a more extensive connection between the ice shelves than the bathymetry product would allow. Furthermore, recent glider and float observations in this region (which are not incorporated into the version of BedMachine used in this study) show that this ridge may be lower than suggested by the gravimetry (Dutrieux et al., 2020). We adjust bathymetry in this region to a maximum of 500 m depth. Our modification of this bathymetry in this region allows a wider area for ocean flow while still maintaining a ridge at the Dotson-Crosson junction. While our modification is not observationally grounded, our adjoint computation (described below) gives an indication of the impact of this modification. If circulation in this region were negligible, such assessment might not be possible.

Our adjoint experiment largely mirrors that of the ISOMIP-bump experiment. Prior to the adjoint run, the Dotson-Crosson model is spun up for 3 years, over the last year of which total melt varies by less than 1%. Beginning with this spun-up state, the adjoint model is run for 1 year, and the sensitivity of the objective function J – the spatial integral of melt – with respect to bathymetry is computed. The realistic experiment was carried out only with the OpenAD-generated adjoint model. Even with the aforementioned adjustments to shorten the required wallclock time of the run, an additional modification to OpenAD was required to circumvent limits on wallclock time on HPC systems. This technical modification is referred to as resilient adjoints and is described in Section 2 of the supplementary material (Aupy et al., 2014; Griewank & Walther, 2000).

4.2 Results

Relevant aspects of the forward model are depicted in Fig. 5. Despite the lower resolution and higher viscosity compared to the configuration used by Goldberg et al. (2019), the melt rate patterns are similar. Broadly consistent with observation-based inferences (Randall-Goodwin et al., 2015), there is a strong outflow at the western margin of Dot-

son Ice Shelf – though in our model outflow is less confined to the margin, potentially due to high viscosities or horizontal resolution. The total melt rate is approximately 81.5 Gt/yr (Fig. 6(b)), similar to that found by Randall-Goodwin et al. (2015) for Dotson ice shelf alone in January 2011. Melt rates in the simulation domain are insensitive to bathymetry under much of the Dotson Ice Shelf (Fig. 6(a)), with the exception of the junction with Crosson Ice Shelf and over the small ridge at the entrance of the ice shelf (the "outer ridge" labelled in Fig. 6(a)).

The sensitivity pattern over the outer ridge bears similarities to the idealized ISOMIP-bump experiment – with negative sensitivities in the centre of the ridge, indicating a lowering would increase melt, and positive sensitivities at the margins. In the junction between Crosson and Dotson ice shelves, there is a somewhat similar pattern, with negative sensitivities along the crest of the ridge (the "inner ridge" indicated in Fig. 6) and positive sensitivities closer to Bear Peninsula where the bed is slightly deeper. However, this pattern should be regarded with caution due to the modifications made to the bathymetry (Section 4.1, Fig. 5(a)).

The most coherent pattern of sensitivity oceanward of Dotson is in the eastern side of the trough entering the cavity (Fig. 6). The negative sensitivities downslope and positive sensitivities upslope imply that a steepening of the trough margin would amplify the geostrophically driven flow of warm water to the ice shelf, and thus increase melting. This result is corroborated by recent observational and experimental work which highlights the critical role of topography in steering heat to Antarctic ice shelves (Wählin et al., 2020).

Under Crosson Ice Shelf, there are fairly weak but extensive positive sensitivities, indicating raising of the bed would increase melt, which at first seems counter-intuitive. This could arise because the cavity column depth is relatively small (on average, the column depth under Crosson is $\sim$150 m less than under Dotson), meaning a shallower column would bring inflowing CDW closer to the ice shelf. Oceanward of Crosson, there are coherent areas of negative sensitivity, correlating with localized bathymetric highs, indicating that lowering in these regions would increase melt. However, this is not a consistent pattern, as there is a region along the front with positive sensitivities, indicating that in this shallow-bedded region, raising the bed would actually increase melt rates.

4.3 Equilibration of adjoint sensitivities

Although the adjoint model represents a differentiation of all physical processes, this does not guarantee that the adjoint run should capture the dominant linear adjustments associated with bathymetric influence of melt. This is because these adjustments operate over an intrinsic time scale (e.g. Heimbach & Losch, 2012), and it is difficult to know *a priori* if the adjoint run encompasses this scale.

The nature of our adjoint run allows us to evaluate whether this adjustment is captured *a posteriori*. The bathymetry field in the ocean model ultimately affects the model through the partial cell factors h_f (*cf.* Section 2.2), and related factors h_f^w and h_f^s, the fluid-filled portion of cell faces at the southern and western sides of bottom cells. This dependency among the cell factors is set in the initialization of the model. Thus, if the *adjoint sensitivity* fields corresponding to these variables are relatively steady as the adjoint model steps backward in time, then bathymetric sensitivities are *converged*: they would not change significantly with a longer run. In physical terms, this would imply that the length of the simulation is on the order of the time scale of adjustment to perturbations or greater.

Fig. 6(b) shows the Euclidean norm of the $\delta^* h_f$ field, the adjoint sensitivity of h_f, as the adjoint model evolves, which it does backward in time (from month 12 to 0). Similar time series are shown for adjoint fields corresponding to the h_f^w and h_f^s fields. $\delta^* h_f^w$ and $\delta^* h_f^s$ norms have roughly steadied by the end of the adjoint run (month 0), while $\delta^* h_f$ is steadily growing. However, $\delta^* h_f$ only makes a small contribution to bathymetric sensitivity over this time period. Since the vertical faces h_f^w and h_f^s determine horizontal transport in the bottom cells, these results suggest the immediate effect of changing bathymetry is on transport, with a timescale of about a year for the present model. However, partial cell volume, which affects, among other things, the heat content at depth, might have strong impacts on melt rate over much longer time scales, not considered here.

We point out that our ability to evaluate adjoint equilibration in this manner is due to our use of time-invariant controls. In adjoint experiments involving time-varying controls, such as wind forcing or time-evolving boundary conditions (e.g., Heimbach & Losch, 2012), the adjoint sensitivity would not be expected to asymptotically approach a "steady state" in reverse-time.

4.4 Impact of bathymetry product uncertainty

As demonstrated in Goldberg et al. (2019), one application of adjoint sensitivities is in estimating the impact of an alternative data product on the quantity of interest. Recently, a new bathymetric product for Antarctica became available, BedMachine (Morlighem et al., 2020), which differs from that of Millan et al. (2017). In particular, there are large differences within the ice shelf cavities, especially for Dotson (Fig. 7(a)), as the bathymetry of Millan was later updated by using the methodology described in An et al. (2019), which makes use of independent measurements of bathymetry to estimate airborne gravity inversion errors arising from density variations.

In a similar fashion to the idealized finite perturbation experiments in section 3.2, we estimate the impact of using the BedMachine product rather than the Millan product by inputting their difference into Eqn. (3). This formula results in an estimated 10 Gt/yr increase in Dotson and Crosson melt-rates resulting purely from the differences in these two products. It is informative to examine which areas of the ice-shelf cavities actually contribute to this increase. This can be seen from Fig. 7(b), which shows

$$\delta J_i = (\delta R_i)(\delta^* R_i) \tag{4}$$

i.e. the summand of Eqn. (3), for this combination of bathymetric perturbation and adjoint sensitivity. Despite the extensive differences in bathymetry under Dotson between the products, there are only a few regions where this difference matters, which are elucidated by the sensitivity pattern in Fig. 6. Most prominently, the representation of the ridge near the front of Dotson, which is far less pronounced in the BedMachine product, accounts for 4.3 Gt/yr difference in melt-rates (Fig. 7(b)).

Of course, this estimate is only a first order approximation as it assumes that this linear term dominates any higher order (i.e. nonlinear) effects. As in Section 3.2, we compare the perturbation in melt to that predicted by the adjoint-based analysis with the response of the full nonlinear model. To this end we run a forward experiment using BedMachine data interpolated to our grid. As the BedMachine data set is in certain locations deeper than our baseline bathymetry by hundreds of meters, there are additional fluid-filled cells whose properties must be initialised. We assign these cells the initial temperature and salinity of the bottom fluid-filled cell in our baseline simulation.

The resulting melt rate forced by BedMachine bathymetry is 71 Gt/yr, which is 10 Gt/yr less than the baseline simulation – the *opposite* of that predicted by the adjoint-based analysis. It should be kept in mind that this response is a composite of responses to a number of large-scale *features*, such as the lowering of the outer ridge under Dotson ice shelf (Fig. 7(a)). We conduct one additional forward perturbation experiment, in which we replace Millan data with BedMachine data, only within the region indicated in Fig. 7(b), i.e. the outer Dotson ridge. The response is an increase in 3.3 Gt/yr, which compares more favorably with the 4.3 Gt/yr predicted by the adjoint analysis.

Our results suggest that our adjoint approach is not likely to reflect the melt response to bathymetric uncertainty at the regional scale. This is not a complete surprise as the adjoint model provides sensitivities linearized about a reference state – in our case, the ocean state given the Millan bathymetry – and changes across the entire model domain of O(100m) are not likely to be captured within a linear regime. On the other hand, we find it encouraging that our model reasonably predicts the response to somewhat more localized perturbations, such as the lowering of the outer ridge under Dotson as shown here. Moreover, we posit that the adjoint model can be a useful tool for identifying these important features, so that the underlying causal drivers can be readily explored in a targeted effort.

4.5 Sensitivity of grounded ice loss to ocean bathymetry

Understanding the impact of ocean bathymetry on sub-ice shelf melt rates is important due to the impact of melting on the loss of buttressing and grounded ice volume (i.e. the volume of ice that can contribute to sea level, Bamber et al. (2018)). The experiments above focus on melt rate as a target quantity of interest, rather than grounded ice volume. To comprehensively estimate sensitivity of grounded ice volume to ocean and sub-ice sheet bathymetric uncertainty would require the adjoint to a fully coupled ice sheet-ocean model, which does not presently exist.

Nevertheless, with our current framework we can begin to explore pathways of sensitivity from ocean model inputs to ice-sheet state-related quantities of interest. In mathematical terms, we seek the total sensitivity of ice sheet volume (as our quantity of interest) to bathymetry, that is, $\frac{\partial V}{\partial R_i}$ where V is grounded ice volume and R is bathymetry in location i. We emphasize that this quantity is distinct from sensitivity of grounded

volume to under-ice bathymetry, which directly controls ice flow and dynamic thinning; rather, the pathway of influence considered here is through control on melt rates, which in turn impact ice-shelf buttressing (see illustration in Fig. 8(a)). Thus, for ocean bathymetric grid points, R_i, we may write:

$$\frac{\partial V}{\partial R_i} = \sum_k \frac{\partial V}{\partial m_k} \frac{\partial m_k}{\partial R_i} \ . \tag{5}$$

where m_k is ocean melt rate in cell k and $\frac{\partial V}{\partial m_k}$ is the ice-sheet model derivative of grounded volume with respect to melt in cell k. While calculating sensitivity of grounded ice volume to melt is beyond the scope of an ocean model, an ice-sheet model framework to do this does exist (e.g., Goldberg & Heimbach, 2013). If these sensitivities can be found, then a new quantity of interest for the ocean model can be defined:

$$J_{gv} = \left(\nabla_{\mathbf{m}} V\right)^T \mathbf{m} \equiv \sum_k \left(\frac{\partial V}{\partial m_k}\right) m_k, \tag{6}$$

Note that if the first term in the inner product is external to the ocean model, then the gradient of J_{gv} with respect to R_i, ocean bathymetry in location i, is equivalent to the expression on the right hand side of Eqn. (5). A different way of seeing this is that the product "projects" patterns of ice sheet volume sensitivities to melt rates onto melt rate sensitivities to ocean bottom topography.

In Goldberg et al. (2019), an *ice-sheet* adjoint model was used to find the sensitivity of grounded volume of Smith Glacier, the glacier that feeds Dotson and Crosson Ice Shelves, to ice-shelf melt rates (Fig. 8(b)). These ice-melt sensitivities are used to construct the quantity of interest J_{gv} and sensitivities with respect to ocean bathymetry are found. This result is shown in Fig. 8(c). The most striking feature of this result is the similarity of the pattern to that of Fig. 6, the sensitivity of melt to bathymetry (R^2 of 0.93; see also Fig. 8(d)). Comparing Eqns. (1) and (6), the quantities of interest effectively differ only in a weighting of melt rate by grounded ice volume sensitivities. Thus the similarity in Figs. 8(c) and 6 suggests that only *total*, or spatially integrated, melt can be strongly affected by bathymetry; whereas melt rate *patterns* are controlled by other factors such as ice-shelf geometry (Goldberg et al., 2019).

We point out this sequence of adjoint sensitivity calculations, in which ice-sheet sensitivity is passed to an ocean model adjoint, which is in turn used to find ocean sensitivity, is a simplified representation of a coupled adjoint ice-ocean model. In a properly coupled model, the ocean provides melt rates to the ice sheet, while the ice sheet

provides ice-shelf drafts to the ocean model, with these fields being continually updated. Ideally, in a coupled adjoint model melt sensitivities would be passed to the ocean adjoint model and ice-draft sensitivities to the ice adjoint model with the same frequency. (In our study, ice-draft sensitivities were not calculated, but our framework could be easily modified to do so.) Moreover, if the ocean and ice models are not on the same grid (as is the case with our ocean model and the ice-sheet model used by Goldberg et al. (2019)), a coupled model would interpolate the melt rates to the ice-sheet grid. Strictly, the term $(\nabla_{\mathbf{m}} V)^T$ in the definition of J_{gv} should be right-multiplied by the adjoint of this interpolation operator. This was not done in our calculation, rather the ice-sheet adjoint sensitivity was interpolated to the ocean grid directly. Still, our results present a useful preliminary assessment of the controls of ocean bathymetry on ice-sheet volume, and can potentially inform more comprehensive assessments using coupled ice sheet-ocean models.

5 Discussion and Conclusions

In this study we have applied an algorithmic differentiation (AD) framework to an ocean general circulation model in order to determine the sensitivity of ice-shelf melt rates to ocean bathymetry. A similar framework of inferring bottom topography sensitivities has been applied before (Losch & Heimbach, 2007), in a coarse-resolution global-scale model. Here, we extend this computational framework to a regional domain that includes circulation in sub-ice shelf cavities in order to assess the impact of uncertainty in bathymetry, a quantity which cannot be measured under ice-shelves by ship-based methods, on melt rates. Additionally, we have made technical improvements by avoiding the differentiation by the AD tool of the Poisson solver for the implicit free surface and facilitating the use of the tool in high performance computing environments (see supplementary materials, sections 1 and 2). We have done so using an open-source AD tool.

Results from both the idealized and realistic simulations show how bathymetry near and underneath ice-shelves modulate melt-rates. Ocean-ward of an ice shelf, troughs leading to the ice front act as a guide for incoming warm ocean waters. Specifically, we show that steepening the trough in front of the Dotson ice shelf would increase melting as a result of increasing the geostrophic inflow. These results provide a complementary perspective to the observations and experimental results shown in Wählin et al. (2020).

Underneath ice shelves, it is well known that ridges or sills hinder the inflow of warm, dense waters into cavities (Dutrieux et al., 2014; De Rydt et al., 2014; Slater et al., 2019; Zhao et al., 2018). However, the spatial details of how these obstacles impact ice shelf melting are in some instances counter-intuitive. For example, the sensitivities in our idealised ISOMIP-bump experiment identified locations where *raising* the level of a sub-ice-shelf ridge led to increased melt. These results were proven to be robust in forward experiments, and they were mirrored in our Dotson-Crosson regional simulation. Thus, while bathymetric obstacles do play a strong role, they do not simply serve as a "dam" to hold back dense warm waters; rather, an obstacle's impact on melt must be assessed in the context of the broader ocean circulation and topographic steering of that circulation.

When calculating sensitivities to bathymetry, the MITgcm adjoint is subject to non-linearities and non-differentiable operators, and may over- or under-estimate response to some perturbations (*cf.* Fig. 3(b)), particularly in response to large perturbations (Section 4.4). More work is needed to determine under what conditions and scales the predicted melt response to bathymetric perturbations is valid. Nevertheless, our idealized experiments suggest the adjoint is able to identify locations and regions where topography "matters". Losch & Heimbach (2007) reach a similar conclusion with their study. They attribute this to low model resolution, though based on our idealised experiments this limitation might apply to high-resolution studies as well.

Regardless, such experiments provide utility to observations of sub-shelf bathymetry which seek to aid modelling of ice-ocean interactions. High-resolution studies of ice-shelf bathymetry (for instance, through gravity analysis and seismic inversion) are possible, but are very limited in scope. As our understanding of sub-shelf bathymetry evolves, our adjoint-based method could be adapted to identify candidate locations where high resolution observational campaigns can be most impactful – for instance, by assessing the potential information gain in important quantities of interest, as in Loose et al. (2020). Additionally, patterns of spatial variability in sensitivity (such as that seen on the flank of Dotson trough) could inform requirements for airborne gravity surveys (in terms of aircraft speed and altitude) to ensure such variability is captured.

A major use of the MITgcm adjoint model is for improved assimilation of oceanographic data (e.g., Wunsch & Heimbach, 2007; Wunsch et al., 2009). However, it is un-

likely that an adjoint ocean model can be used to estimate sub-ice shelf bathymetry by assimilating spatial observations of melt rates, for two reasons. Firstly, as demonstrated in our idealised and realistic experiments, there are extensive regions under ice shelves where melt rates are not sensitive to bathymetry. Thus two very different bathymetry products (such as the Millan and BedMachine datasets) could give very similar melt rates. Secondly, sub-shelf circulation seems to "filter" the effects on melt rate, such that while bathymetry has a strong impact on total melt, its effect on melt rate patterns may be weaker – effectively limiting the information contained in spatially resolved melt patterns (Gourmelen et al., 2017). It may be possible, nevertheless, to "fine tune" our knowledge of bathymetry in regions that are known to strongly impact melt rates.

Our study was spatially limited in that only Crosson and Dotson ice shelves were modelled – but it was also *temporally* limited, with time-invariant conditions representing far-field heat content and thermocline depths. In reality, the depth of CDW on the Amundsen shelf and elsewhere in Antarctica varies both seasonally and interannually (e.g., Thoma et al., 2008; Jenkins et al., 2016; Webber et al., 2017), and it is possible that this variability could impact sensitivity of melt to bathymetry. Furthermore, our choice of resolution and horizontal viscosity may have precluded resolution of turbulent eddies which interact with bathymetry, affecting transport of heat to the ice-ocean interface. Therefore, the results in Section 4 should be viewed as a preliminary exploration of bathymetric sensitivity of ice-shelf melt for Antarctic ice shelves. Our methodology must be applied to simulations of ice-ocean interactions that are longer-term, more spatially extensive, and validated against observations of ice-shelf melt (Rignot et al., 2013; Gourmelen et al., 2017; Jenkins et al., 2018) in order that the impacts of ocean bathymetry upon ice-shelf melt can be fully evaluated.

The full potential of this work may be realised in fully coupled forward and adjoint ocean-ice sheet calculations on decadal to century scales, in which ice sheet volume sensitivities to ocean bathymetric uncertainties may be more comprehensively studied. To do so will require tackling computational challenges along two main fronts. The first is in terms of efficient, property-conserving strategies allowing century-scale coupled ice-ocean simulations at resolutions that resolve important oceanographic phenomena, using codes that are adjoinable. Some progress has already been made in this area through decadal-scale synchronous coupling of the MITgcm ocean and land ice models (Jordan

et al., 2017; Goldberg et al., 2018), both of which have been differentiated by both TAF and OpenAD.

The second front is in terms of the efficiency of the adjoint model relative to the forward model. Adjoint models are extremely efficient in terms of sensitivity analyses, providing ability to estimate sensitivity to tens or hundreds of thousands of input parameters simultaneously. However, model nonlinearities require that intermediate variables be stored or recomputed because of the time-reversed adjont integration. As a result the adjoint run time is generally a multiple of the forward model. Certain AD tools such as TAF have achieved multiples on the order of 3 to 6 – but this performance is a result of extensive performance optimization of these tools in relation to the application code, and this multiple can vary by an order of magnitude among any AD tool which has not been similarly optimized, such as OpenAD. Therefore achieving performance in the open-source domain that would make large-scale adjoint studies of coupled ice-ocean dynamics feasible requires further close collaboration between domain scientists and developers of AD software.

Acknowledgments and Code/Data Availability.

D.G. was supported by NERC Standard Grants NE/M003590/1 and NE/T001607/1. D.G. and M.M. were supported jointly by NERC-NSF ITGC Grant PROPHET. T.S. and P.H. were supported in part by NSF grant #1750035 and JPL/Caltech subcontract "ECCO: Understanding Sea Level, Ice, and Earths Climate". S.N. was supported by the U.S. Department of Energy, Office of Science, under contract DE-AC02-06CH11357. MITgcm code can be accessed publicly at mitgcm.org and OpenAD from https://www.mcs.anl.gov/OpenAD. BedMachine data is available from https://nsidc.org/data/nsidc-0756 . Output availability information for Kimura et al. (2017) is given in their publication. All model output used to produce figures for this manuscript is provided as supporting information.

References

Adcroft, A., Hill, C., & Marshall, J. (1997). Representation of topography by shaved cells in a height coordinate ocean model. Monthly Weather Review, 125(9), 2293-2315. doi: 10.1175/1520-0493(1997)125

An, L., Rignot, E., Millan, R., Tinto, K., & Willis, J. (2019). Bathymetry of North-

west Greenland Using "Ocean Melting Greenland" (OMG) High-Resolution Airborne Gravity and Other Data. Remote Sens., 11(2). Retrieved from https://www.mdpi.com/2072-4292/11/2/131 doi: 10.3390/rs11020131

Arneborg, L., Wåhlin, A. K., Björk, G., Liljebladh, B., & Orsi, A. H. (2012, Nov 25). Persistent inflow of warm water onto the central amundsen shelf. Nature Geoscience, 5, 876–880. doi: 10.1038/ngeo1644

Aupy, G., Herrmann, J., Hovland, P., & Robert, Y. (2014, 04). Optimal multistage algorithm for adjoint computation. SIAM Journal on Scientific Computing, 38. doi: 10.1137/15M1019222

Bamber, J. L., Westaway, R. M., Marzeion, B., & Wouters, B. (2018, jun). The land ice contribution to sea level during the satellite era. Environmental Research Letters, 13(6), 063008. doi: 10.1088/1748-9326/aac2f0

Bentley, C. R., Crary, A. P., Ostenso, N. A., & Thiel, E. C. (1960, January). Structure of West Antarctica. Science, 131(3394), 131–136.

Cochran, J. R., & Bell, R. E. (2012). Inversion of icebridge gravity data for continental shelf bathymetry beneath the larsen ice shelf, antarctica. Journal of Glaciology, 58(209), 540–552. doi: 10.3189/2012JoG11J033

Dansereau, V., Heimbach, P., & Losch, M. (2014). Simulation of subice shelf melt rates in a general circulation model: Velocity-dependent transfer and the role of friction. Journal of Geophysical Research: Oceans, 119(3), 1765–1790. Retrieved from http://dx.doi.org/10.1002/2013JC008846 doi: 10.1002/2013JC008846

De Rydt, J., Holland, P. R., Dutrieux, P., & Jenkins, A. (2014). Geometric and oceanographic controls on melting beneath pine island glacier. Journal of Geophysical Research: Oceans, 119(4), 2420–2438. Retrieved from http://dx.doi.org/10.1002/2013JC009513 doi: 10.1002/2013JC009513

Dutrieux, P., De Rydt, J., Jenkins, A., Holland, P., Ha, H., Lee, S., ... Schröder, M. (2014). Strong sensitivity of pine island ice-shelf melting to climatic variability. Science, 343(6167), 174–178. Retrieved from http://science.sciencemag.org/content/343/6167/174 doi: 10.1126/science.1244341

Dutrieux, P., Lee, C., Rainville, L., Gobat, J., Girton, J., Christianson, K., ... Millan, R. (2020). Seaglider and Float Observations Beneath Dotson Ice Shelf, West Antarctica. In Ocean sciences meeting abstracts.

Errico, R. M. (1997). What is an adjoint model? BAMS, 78, 2577–2591.

Gerringa, L. J., Alderkamp, A.-C., Laan, P., Thur'oczy, C.-E., Baar, H. J. D., Mills, M. M., ... Arrigo, K. R. (2012). Iron from melting glaciers fuels the phytoplankton blooms in amundsen sea (southern ocean): Iron biogeochemistry. Deep Sea Research Part II: Topical Studies in Oceanography, 71-76, 16 - 31. Retrieved from http://www.sciencedirect.com/science/article/pii/S0967064512000446 doi: https://doi.org/10.1016/j.dsr2.2012.03.007

Giering, R., Kaminski, T., & Slawig, T. (2005, October). Generating efficient derivative code with TAF adjoint and tangent linear euler flow around an airfoil. Future Gener. Comput. Syst., 21(8), 1345–1355. Retrieved from http://dx.doi.org/10.1016/j.future.2004.11.003 doi: 10.1016/j.future.2004.11.003

Giles, M. B., Corliss, G., Faure, C., Griewank, A., Hascoët, L., & Naumann, U. (2002). On the iterative solution of adjoint equations. In Automatic differentiation of algorithms: From simulation to optimization (pp. 145–151). New York, NY: Springer New York. doi: 10.1007/978-1-4613-0075-5-16

Gille, S. T., Metzger, E. J., & Tokmakian, R. (2004, March). Seafloor topography and ocean circulation. Oceanography, 17. Retrieved from https://doi.org/10.5670/oceanog.2004.66

Goldberg, D., Gourmelen, N., Kimura, S., Millan, R., & Snow, K. (2019). How accurately should we model ice shelf melt rates? Geophysical Research Letters, 46(1), 189-199. Retrieved from https://agupubs.onlinelibrary.wiley.com/doi/abs/10.1029/2018GL080383 doi: 10.1029/2018GL080383

Goldberg, D., & Heimbach, P. (2013). Parameter and state estimation with a time-dependent adjoint marine ice sheet model. The Cryosphere, 7(6), 1659–1678. Retrieved from http://www.the-cryosphere.net/7/1659/2013/ doi: 10.5194/tc-7-1659-2013

Goldberg, D., Heimbach, P., Joughin, I., & Smith, B. (2015). Committed retreat of smith, pope, and kohler glaciers over the next 30 years inferred by transient model calibration. The Cryosphere, 9(6), 2429–2446. Retrieved from https://www.the-cryosphere.net/9/2429/2015/ doi: 10.5194/tc-9-2429-2015

Goldberg, D., Snow, K., Holland, P., Jordan, J., Campin, J.-M., Heimbach, P., ... Jenkins, A. (2018). Representing grounding line migration in synchronous coupling between a marine ice sheet model and a z-coordinate ocean model. Ocean Modelling, 125, 45 - 60. Retrieved from http://www.sciencedirect.com/

science/article/pii/S1463500318301021 doi: https://doi.org/10.1016/j.ocemod.2018.03.005

Gourmelen, N., N., G. D., Kate, S., F., H. S., G., B. R., Satoshi, K., ... Jan, B. W. (2017). Channelized melting drives thinning under a rapidly melting antarctic ice shelf. Geophysical Research Letters, 44(19), 9796-9804. Retrieved from https://agupubs.onlinelibrary.wiley.com/doi/abs/10.1002/2017GL074929 doi: 10.1002/2017GL074929

Graham, J. A., Dinniman, M. S., & Klinck, J. M. (2016). Impact of model resolution for on-shelf heat transport along the west antarctic peninsula. Journal of Geophysical Research: Oceans, 121(10), 7880-7897. Retrieved from https://agupubs.onlinelibrary.wiley.com/doi/abs/10.1002/2016JC011875 doi: 10.1002/2016JC011875

Greene, C. A., Blankenship, D. D., Gwyther, D. E., Silvano, A., & van Wijk, E. (2017). Wind causes totten ice shelf melt and acceleration. Science Advances, 3(11). Retrieved from https://advances.sciencemag.org/content/3/11/e1701681 doi: 10.1126/sciadv.1701681

Griewank, A., & Walther, A. (2000, March). Algorithm 799: Revolve: An implementation of checkpointing for the reverse or adjoint mode of computational differentiation. ACM Trans. Math. Softw., 26(1), 19–45. Retrieved from http://doi.acm.org/10.1145/347837.347846 doi: 10.1145/347837.347846

Griewank, A., & Walther, A. (2008). Evaluating derivatives. principles and techniques of algorithmic differentiation, vol. 19 of frontiers in applied mathematics (2nd ed.). Philadelphia: SIAM.

Gwyther, D. E., Galton-Fenzi, B. K., Hunter, J. R., & Roberts, J. L. (2014). Simulated melt rates for the totten and dalton ice shelves. Ocean Science, 10(3), 267–279. Retrieved from http://www.ocean-sci.net/10/267/2014/ doi: 10.5194/os-10-267-2014

Heimbach, P., Hill, C., & Giering, R. (2005). An efficient exact adjoint of the parallel MIT general circulation model, generated via automatic differentiation. Future Generation Computer Systems, 21, 1356–1371.

Heimbach, P., & Losch, M. (2012). Adjoint sensitivities of sub-ice shelf melt rates to ocean circulation under Pine Island Ice Shelf, West Antarctica. Annals of Glaciol., 54, 59–69. doi: 10.3189/2012/AoG60A025

Heimbach, P., Wunsch, C., Ponte, R. M., Forget, G., Hill, C., & Utke, J. (2011). Timescales and regions of the sensitivity of atlantic meridional volume and heat transport: Toward observing system design. Deep Sea Research Part II: Topical Studies in Oceanography, 58(17), 1858 - 1879. Retrieved from http://www.sciencedirect.com/science/article/pii/S0967064511000488 (Climate and the Atlantic Meridional Overturning Circulation) doi: https://doi.org/10.1016/j.dsr2.2010.10.065

Hellmer, H. H., Kauker, F., Timmermann, R., Determann, J., & Rae, J. (2012). Twenty-first-century warming of a large antarctic ice-shelf cavity by a redirected coastal current. Nature, 485(7397), 225-228. Retrieved from https://doi.org/10.1038/nature11064 doi: 10.1038/nature11064

Holland, D. M., Hunter, J., Grosfeld, K., Hellmer, H., Jenkins, A., Morales Maqueda, M. A., ... Dinniman, M. (2003, December). The Ice Shelf - Ocean Model Intercomparison Project (ISOMIP). AGU Fall Meeting Abstracts, C41A-05.

Holland, D. M., Jacobs, S. S., & Jenkins, A. (2003). Modelling the ocean circulation beneath the Ross Ice Shelf. Antarctic Science, 15, 13–23.

Holland, D. M., & Jenkins, A. (1999). Modelling thermodynamic ice-ocean interactions at the base of an ice shelf. J. Phys. Ocean., 29, 1787–1800. doi: https://doi.org/10.1175/1520-0485(1999)029

Hoteit, I., Cornuelle, B., Köhl, A., & Stammer, D. (2005). Treating strong adjoint sensitivities in tropical eddy-permitting variational data assimilation. Quarterly Journal of the Royal Meteorological Society, 131(613), 3659–3682. Retrieved 2019-10-21, from https://rmets.onlinelibrary.wiley.com/doi/abs/10.1256/qj.05.97 doi: 10.1256/qj.05.97

Hughes, C. W., & Killworth, P. D. (1995). Effects of bottom topography in the large-scale circulation of the southern ocean. Journal of Physical Oceanography, 25(11), 2485-2497. Retrieved from https://doi.org/10.1175/1520-0485(1995)025<2485:EOBTIT>2.0.CO;2 doi: 10.1175/1520-0485(1995)025⟨2485:EOBTIT⟩2.0.CO;2

Huppert, H. E., & Bryan, K. (1976). Topographically generated eddies. Deep Sea Research and Oceanographic Abstracts, 23(8), 655 - 679. Retrieved from http://www.sciencedirect.com/science/article/pii/S0011747176800137

805 doi: https://doi.org/10.1016/S0011-7471(76)80013-7

806 Jacobs, S. S., Hellmer, H., & Jenkins, A. (1996). Antarctic ice sheet melting in the
807 Southeast Pacific. Geophys. Res. Lett., 23, 957–960. doi: https://doi.org/10.1175/
808 1520-0485(1999)029

809 Jacobs, S. S., Jenkins, A., Giulivi, C., & Dutrieux, P. (2011). Stronger ocean circu-
810 lation and increased melting under Pine Island Glacier ice shelf. Nat. Geosci.. doi:
811 10.1038/NGEO1188

812 Jenkins, A. (2016). A simple model of the ice shelf-ocean boundary layer and
813 current. Journal of Physical Oceanography, 46(6), 1785-1803. Retrieved from
814 http://dx.doi.org/10.1175/JPO-D-15-0194.1 doi: 10.1175/JPO-D-15-0194.1

815 Jenkins, A., Dutrieux, P., Jacobs, S., Steig, E. J., Gudmundsson, H., Smith, J.,
816 & Heywood, K. (2016, December). Decadal ocean forcing and antarctic ice
817 sheet response: Lessons from the amundsen sea. Oceanography, 29. doi:
818 https://doi.org/10.5670/oceanog.2016.103

819 Jenkins, A., Dutrieux, P., Jacobs, S. S., McPhail, S. D., Perrett, J. R., Webb, A. T.,
820 & White, D. (2010). Observations beneath Pine Island Glacier in West Antarctica
821 and implications for its retreat. Nat. Geosci., 3, 468–472.

822 Jenkins, A., & Holland, D. M. (2007). Melting of floating ice and sea level rise.
823 Geophys. Res. Lett., 34, L16609.

824 Jenkins, A., Shoosmith, D., Dutrieux, P., Jacobs, S., Kim, T. W., Le, S. H., ...
825 Stammerjohn, S. (2018). West antarctic ice sheet retreat in the amundsen
826 sea driven by decadal oceanic variability. Nat. Geoscience, 11, 733–738. doi:
827 https://doi.org/10.1038/s41561-018-0207-4DO

828 Jenkins, A., Vaughan, D. G., Jacobs, S. S., Hellmer, H. H., & Keys, J. R. (1997).
829 Glaciological and oceanographic evidence of high melt rates beneath Pine Island
830 Glacier, West Antarctica. Journal of Glaciology, 43(143), 114–121.

831 Jordan, J. R., Holland, P. R., Goldberg, D., Snow, K., Arthern, R., Campin, J.-M.,
832 ... Jenkins, A. (2017). Ocean-forced ice-shelf thinning in a synchronously coupled
833 ice-ocean model. Journal of Geophysical Research: Oceans, n/a–n/a. Retrieved
834 from http://dx.doi.org/10.1002/2017JC013251 doi: 10.1002/2017JC013251

835 Joughin, I., Smith, B. E., & Medley, B. (2014). Marine ice sheet collapse potentially
836 under way for the Thwaites Glacier Basin, West Antarctica. Science, 344(6185),
837 735-738. Retrieved from http://www.sciencemag.org/content/344/6185/735

.abstract doi: 10.1126/science.1249055

Kimura, S., Adrian, J., Heather, R., R., H. P., M., A. K., B., W. D., ... Pierre, D. (2017). Oceanographic controls on the variability of ice-shelf basal melting and circulation of glacial meltwater in the amundsen sea embayment, antarctica. Journal of Geophysical Research: Oceans, 122(12), 10131-10155. Retrieved from https://agupubs.onlinelibrary.wiley.com/doi/abs/10.1002/2017JC012926 doi: 10.1002/2017JC012926

Lilien, D. A., Joughin, I., Smith, B., & Shean, D. E. (2018). Changes in flow of crosson and dotson ice shelves, west antarctica, in response to elevated melt. The Cryosphere, 12(4), 1415–1431. Retrieved from https://www.the-cryosphere.net/12/1415/2018/ doi: 10.5194/tc-12-1415-2018

Loose, N., Heimbach, P., Pillar, H. R., & Nisancioglu, K. H. (2020). Quantifying dynamical proxy potential through shared adjustment physics in the north atlantic. Journal of Geophysical Research: Oceans, 125(9), e2020JC016112. Retrieved from https://agupubs.onlinelibrary.wiley.com/doi/abs/10.1029/2020JC016112 (e2020JC016112 10.1029/2020JC016112) doi: 10.1029/2020JC016112

Losch, M. (2008). Modeling ice shelf cavities in a z coordinate ocean general circulation model. Journal of Geophysical Research: Oceans, 113(C8), n/a–n/a. Retrieved from http://dx.doi.org/10.1029/2007JC004368 doi: 10.1029/2007JC004368

Losch, M., & Heimbach, P. (2007). Adjoint sensitivity of an ocean general circulation model to bottom topography. Journal of Physical Oceanography, 37(2), 377-393. Retrieved from https://doi.org/10.1175/JPO3017.1 doi: 10.1175/JPO3017.1

Marshall, D. (1995). Influence of topography on the large-scale ocean circulation. Journal of Physical Oceanography, 25(7), 1622-1635. Retrieved from https://doi.org/10.1175/1520-0485(1995)025<1622:IOTOTL>2.0.CO;2 doi: 10.1175/1520-0485(1995)025⟨1622:IOTOTL⟩2.0.CO;2

Marshall, J., Hill, C., Perelman, L., & Adcroft, A. (1997). Hydrostatic, quasi-hydrostatic, and nonhydrostatic ocean modeling. Journal of Geophysical Research: Oceans, 102(C3), 5733–5752. Retrieved from http://dx.doi.org/10.1029/96JC02776 doi: 10.1029/96JC02776

Mathiot, P., Jenkins, A., Harris, C., & Madec, G. (2017). Explicit represen-

tation and parametrised impacts of under ice shelf seas in the z^* coordinate ocean model nemo 3.6. Geoscientific Model Development, 10(7), 2849–2874. Retrieved from https://www.geosci-model-dev.net/10/2849/2017/ doi: 10.5194/gmd-10-2849-2017

Miles, T., Lee, S. H., Wåhlin, A., Ha, H. K., Kim, T. W., Assmann, K. M., & Schofield, O. (2016). Glider observations of the Dotson Ice Shelf outflow. Deep Sea Research Part II: Topical Studies in Oceanography, 123, 16 - 29. Retrieved from http://www.sciencedirect.com/science/article/pii/S096706451500301X doi: https://doi.org/10.1016/j.dsr2.2015.08.008

Millan, R., Rignot, E., Bernier, V., Morlighem, M., & Dutrieux, P. (2017). Bathymetry of the Amundsen Sea Embayment sector of West Antarctica from Operation IceBridge gravity and other data. Geophysical Research Letters, 44(3), 1360-1368. doi: 10.1002/2016GL072071

Morlighem, M., Rignot, E., Binder, T., Blankenship, D., Drews, R., & others, . (2020). Deep glacial troughs and stabilizing ridges unveiled beneath the margins of the antarctic ice sheet. Nature Geoscience, 13(2), 132–137. doi: 10.1038/s41561-019-0510-8

Nitsche, F. O., Jacobs, S. S., Larter, R. D., & Gohl, K. (2007). Bathymetry of the amundsen sea continental shelf: Implications for geology, oceanography, and glaciology. Geochemistry, Geophysics, Geosystems, 8(10). Retrieved from https://agupubs.onlinelibrary.wiley.com/doi/abs/10.1029/2007GC001694 doi: 10.1029/2007GC001694

Padman, L., Costa, D. P., Bolmer, S. T., Goebel, M. E., Huckstadt, L. A., Jenkins, A., ... Shoosmith, D. R. (2010). Seals map bathymetry of the antarctic continental shelf. Geophysical Research Letters, 37(21). doi: 10.1029/2010GL044921

Petty, A. A., Feltham, D. L., & Holland, P. R. (2013). Impact of Atmospheric Forcing on Antarctic Continental Shelf Water Masses. Journal of Physical Oceanography, 43(5), 920-940. Retrieved from https://doi.org/10.1175/JPO-D-12-0172.1 doi: 10.1175/JPO-D-12-0172.1

Pillar, H. R., Heimbach, P., Johnson, H. L., & Marshall, D. P. (2016, February). Dynamical Attribution of Recent Variability in Atlantic Overturning. Journal of Climate, 29(9), 3339–3352. Retrieved 2019-09-04, from https://journals.ametsoc.org/doi/full/10.1175/JCLI-D-15-0727.1 doi:

10.1175/JCLI-D-15-0727.1

Pritchard, H. D., Ligtenberg, S. R. M., Fricker, H. A., Vaughan, D. G., van den Broeke, M. R., & Padman, L. (2012, April). Antarctic ice-sheet loss driven by basal melting of ice shelves. Nature, 484(7395), 502–505.

Randall-Goodwin, E., Meredith, M. P., Jenkins, A., Yager, P. L., Sherrell, R. M., Abrahamsen, E. P., ... Stammerjohn, S. E. (2015). Freshwater distributions and water mass structure in the Amundsen Sea Polynya region, Antarctica. Elementa, 5, 65. doi: http://doi.org/10.12952/journal.elementa.000065

Rignot, E., Jacobs, S., Mouginot, J., & Scheuchl, B. (2013). Ice-Shelf Melting Around Antarctica. Science, 341(6143), 266–270. Retrieved from `http://science.sciencemag.org/content/341/6143/266` doi: 10.1126/science.1235798

Roberts, M. J., & Wood, R. A. (1997). Topographic sensitivity studies with a bryan–cox-type ocean model. Journal of Physical Oceanography, 27(5), 823-836. Retrieved from `https://doi.org/10.1175/1520-0485(1997)027<0823:TSSWAB>2.0.CO;2` doi: 10.1175/1520-0485(1997)027⟨0823:TSSWAB⟩2.0.CO;2

Rosier, S. H. R., Hofstede, C., Brisbourne, A. M., Hattermann, T., Nicholls, K. W., Davis, P. E. D., ... Corr, H. F. J. (2018). A new bathymetry for the southeastern filchner-ronne ice shelf: Implications for modern oceanographic processes and glacial history. Journal of Geophysical Research: Oceans, 123(7), 4610-4623. doi: 10.1029/2018JC013982

Schodlok, M. P., Menemenlis, D., Rignot, E., & Studinger, M. (2012). Sensitivity of the ice-shelf/ocean system to the sub-ice-shelf cavity shape measured by NASA IceBridge in Pine Island Glacier, West Antarctica. Annals of Glaciology, 53(60), 156–162.

Schoof, C. (2007). Marine ice sheet dynamics. Part I. The case of rapid sliding. J. Fluid Mech., 573, 27–55.

Shepherd, A., Wingham, D. J., & Rignot, E. (2004). Warm ocean is eroding West Antarctic Ice Sheet. Geophys. Res. Lett., 31, L23402.

Sirkes, Z., & Tziperman, E. (1997). Finite difference of adjoint or adjoint of finite difference? Monthly Weather Review, 125(12), 3373-3378. doi: 10.1175/1520-0493(1997)

Slater, D. A., Felikson, D., Straneo, F., Goelzer, H., Little, C. M., Morlighem, M., ... Nowicki, S. (2019). 21st century ocean forcing of the greenland ice sheet for

modeling of sea level contribution. The Cryosphere Discussions, 2019, 1–34. Retrieved from https://www.the-cryosphere-discuss.net/tc-2019-222/ doi: 10.5194/tc-2019-222

Smith, T., & Heimbach, P. (2019). Atmospheric Origins of Variability in the South Atlantic Meridional Overturning Circulation. Journal of Climate, 32(5), 1483–1500. Retrieved 2019-02-07, from http://journals.ametsoc.org/doi/10.1175/JCLI-D-18-0311.1 doi: 10.1175/JCLI-D-18-0311.1

Thoma, M., Jenkins, A., Holland, D. M., & Jacobs, S. S. (2008). Modelling Circumpolar Deep Water intrusions on the Amundsen Sea continental shelf, Antarctica. Geophys. Res. Lett., 35. doi: 10.1029/2008GL034939

Thomas, R. H. (1979). The dynamics of marine ice sheets. Journal of Glaciology, 24, 167–177.

Thomas, R. H., & Bentley, C. R. (1978). A model for the Holocene retreat of the West Antarctic Ice Sheet. Quaternary Research, 10, 150–170.

Thompson, A. F., Stewart, A. L., Spence, P., & Heywood, K. J. (2018, December). The Antarctic Slope Current in a Changing Climate. Reviews of Geophysics, 56(4), 741–770.

Tinto, K. J., & Bell, R. E. (2011). Progressive unpinning of thwaites glacier from newly identified offshore ridge: Constraints from aerogravity. Geophysical Research Letters, 38(20), L20503. Retrieved from http://dx.doi.org/10.1029/2011GL049026 doi: 10.1029/2011GL049026

Utke, J., Naumann, U., Fagan, M., Tallent, N., Strout, M., Heimbach, P., ... Wunsch, C. (2008). OpenAD/F: A modular open source tool for automatic differentiation of Fortran codes. ACM Transactions on Mathematical Software, 34.

Wählin, A. K., Steiger, N., Darelius, E., Assmann, K. M., Glessmer, M. S., Ha, H. K., ... Viboud, S. (2020, February). Ice front blocking of ocean heat transport to an Antarctic ice shelf. Nature, 578(7796), 568–571. Retrieved 2020-02-28, from http://www.nature.com/articles/s41586-020-2014-5 (Number: 7796 Publisher: Nature Publishing Group) doi: 10.1038/s41586-020-2014-5

Walker, D. P., Jenkins, A., Assmann, K., Shoosmith, D., & Brandon, M. (2013). Oceanographic observations at the shelf break of the Amundsen Sea, Antarctica. Journal of Geophysical Research: Oceans, 118(6), 2906-2918. Retrieved from https://agupubs.onlinelibrary.wiley.com/doi/abs/10.1002/jgrc.20212

970 doi: 10.1002/jgrc.20212

971 Webber, B., Heywood, K., Stevens, D. P., Dutrieux, P., Abrahamsen, E. P., Jenk-
972 ins, A., ... Kim, T. W. (2017, February). Mechanisms driving variability in the
973 ocean forcing of Pine Island Glacier. Nature Communications, 8, 14507. doi:
974 10.1038/ncomms14507

975 Wei, W., Blankenship, D. D., Greenbaum, J. S., Gourmelen, N., Dow, C. F., Richter,
976 T. G., ... Assmann, K. M. (2019). Getz ice shelf melt enhanced by freshwater
977 discharge from beneath the west antarctic ice sheet. The Cryosphere Discussions,
978 2019, 1–16. Retrieved from https://www.the-cryosphere-discuss.net/
979 tc-2019-170/ doi: 10.5194/tc-2019-170

980 Wunsch, C. (1996). The ocean circulation inverse problem. New York: Cambridge
981 University Press.

982 Wunsch, C., & Heimbach, P. (2007). Practical global ocean state estimation.
983 Physica D, 230, 197–208.

984 Wunsch, C., Ponte, R., Heimbach, P., & Fukumori, I. (2009). The global general
985 circulation of the ocean estimated by the ecco-consortium. Oceanography, 22, 88-
986 103.

987 Yager, P. L., Sherrell, R. M., Stammerjohn, S. E., Alderkamp, A.-C., Schofield, O.,
988 Abrahamsen, E. P., ... Wilson, S. (2012, September). Aspire: The amundsen
989 sea polynya international researchexpedition. Oceanography, 25. Retrieved from
990 https://doi.org/10.5670/oceanog.2012.73

991 Zhang, X., Thompson, A. F., Flexas, M. M., Roquet, F., & Bornemann, H.
992 (2016). Circulation and meltwater distribution in the bellingshausen sea: From
993 shelf break to coast. Geophysical Research Letters, 43(12), 6402-6409. doi:
994 10.1002/2016GL068998

995 Zhao, K. X., Stewart, A. L., & McWilliams, J. C. (2018, November). Sill-Influenced
996 Exchange Flows in Ice Shelf Cavities. Journal of Physical Oceanography, 49(1),
997 163–191. Retrieved 2019-06-05, from https://journals.ametsoc.org/doi/full/
998 10.1175/JPO-D-18-0076.1 doi: 10.1175/JPO-D-18-0076.1

999

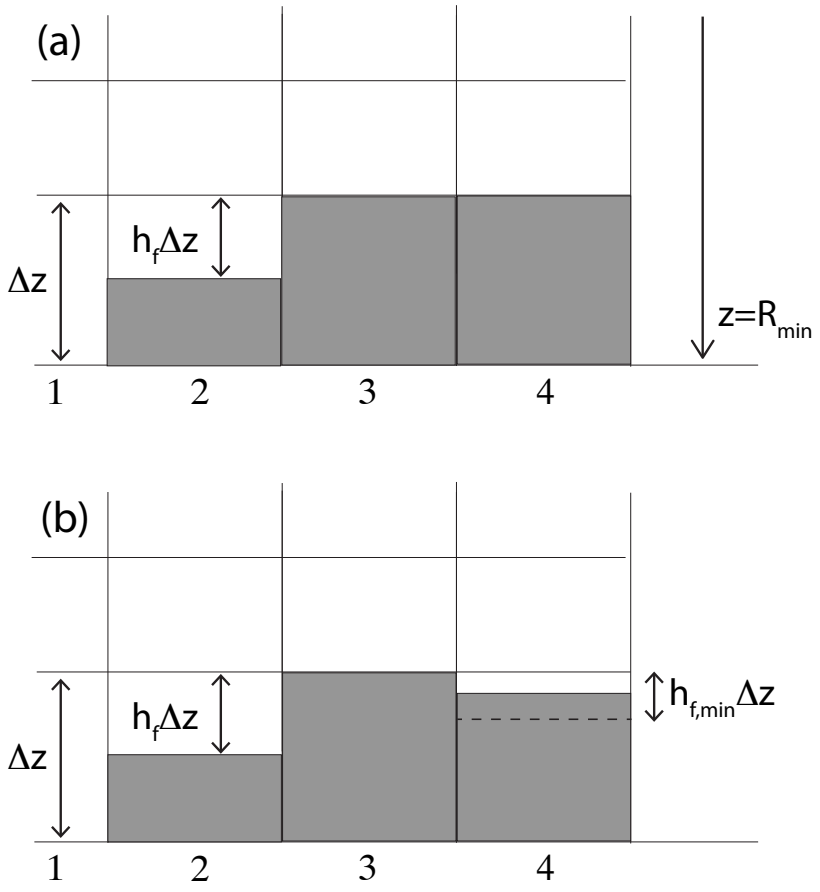

Figure 1. (a) A schematic (adapted from http://mitgcm.org/) of the representation of bottom topography in MITgcm. The white regions within cells contain fluid. In column 1, all cells are fluid-filled and the bathymetry is R_{min}. The bottom cells of Columns 3 and 4 are non-fluid-containing, and in these columns the bottom elevation is $R_{min} + \Delta z$. In Column 2, the bottom cell is a partial cell, and bathymetry is $R_{min} + (1 - h_f)\Delta z$. The interface between the bottom cells of Column 1 and Column 2 has height $h_f \Delta z$, and there is no interface between the bottom cell of Column 2 with any cell in Column 3. (b) A perturbation to bathymetry is made, indicated by gray shading in to bottom cell of Column 4. Depending on the size of the perturbation, ocean model initialisation may lower bathymetry further so that the liquid-containing portion of the bottom cell is $h_{f,min}\Delta z$; or it may restore bathymetry to that of (a).

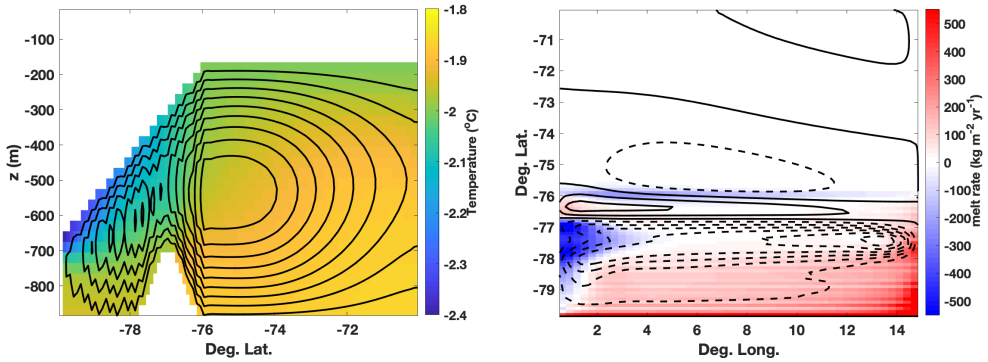

Figure 2. (left) Zonally averaged temperature (shading) and overturning stream function (contours, spacing 0.01 Sv) in the modified ISOMIP experiment. The profile of the "ridge" is apparent between -78° and -76° Latitude. (right) Melt rate at the termination of the experiment (shading; negative values indicate accretion) and depth-integrated stream function (contours, spacing 0.05 Sv; dashed lines where negative).

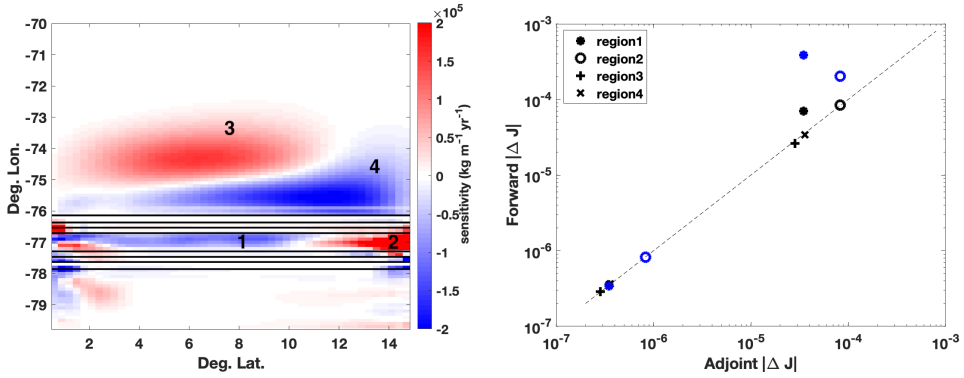

Figure 3. (left) Domain bathymetry (contours; 50m isolines) and sensitivity of spatially-integrated melt at model termination to bathymetry (shading); value of sensitivity in a cell indicates gradient of melt with respect to elevation in the cell, where positive (negative) values indicate regions where raising (lowering) the bottom will increase melt. (right) Comparison of perturbed objective function ("Forward" $|\Delta J|$, in Gt/a melt) with value predicted by linearized sensitivities ("Adjoint" $|\Delta J|$), as described in Section 3.2. Blue markers indicate negative perturbations while black markers indicate positive ones. Small values (less than 10^{-6} Gt/a) indicate perturbations scaled by 0.1m and large values (greater than 10^{-5} Gt/a) indicate perturbations scaled by 10m. Though the *sign* of the observed ΔJ is not given, it is in all cases the same as the prediction.

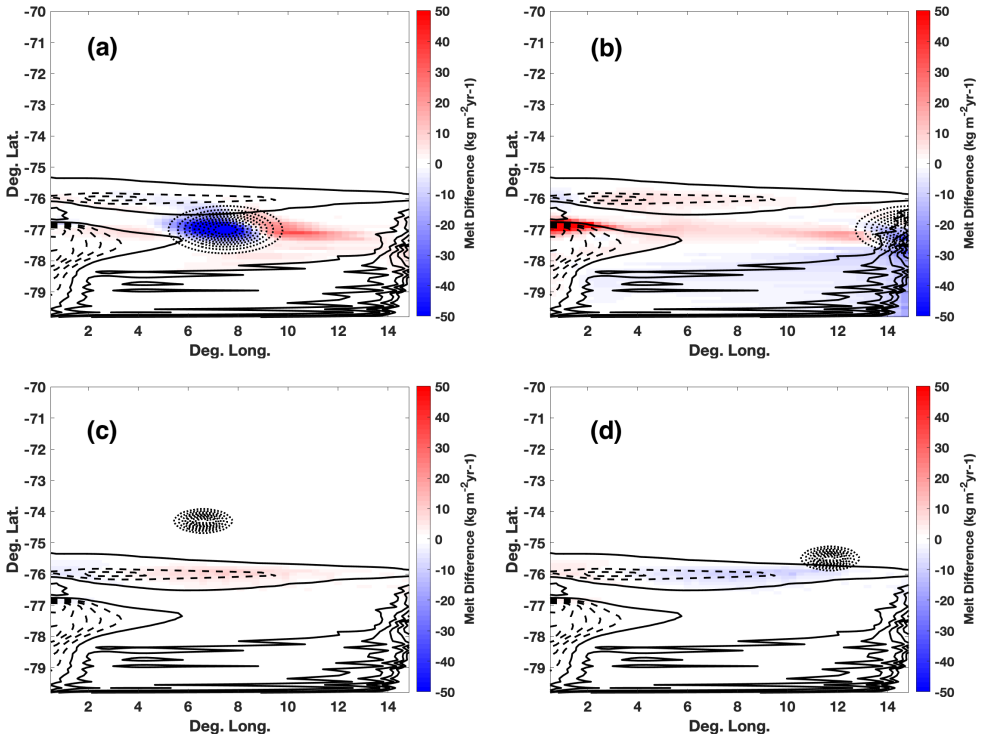

Figure 4. Perturbed beds (dotted contours) and corresponding perturbed melt rates (shading) in different regions of high sensitivity in Fig. 3. (a) through (d) correspond to finite perturbations in locations (1) through (4) in Fig. 3(a), respectively. Bathymetric peturbations plotted with δR=10 (Eqn. 3) and 1m isolines. Isolines of unperturbed melt rates are also shown (solid where positive, dashed where negative; 100 kg m^{-2}yr^{-1} spacing).

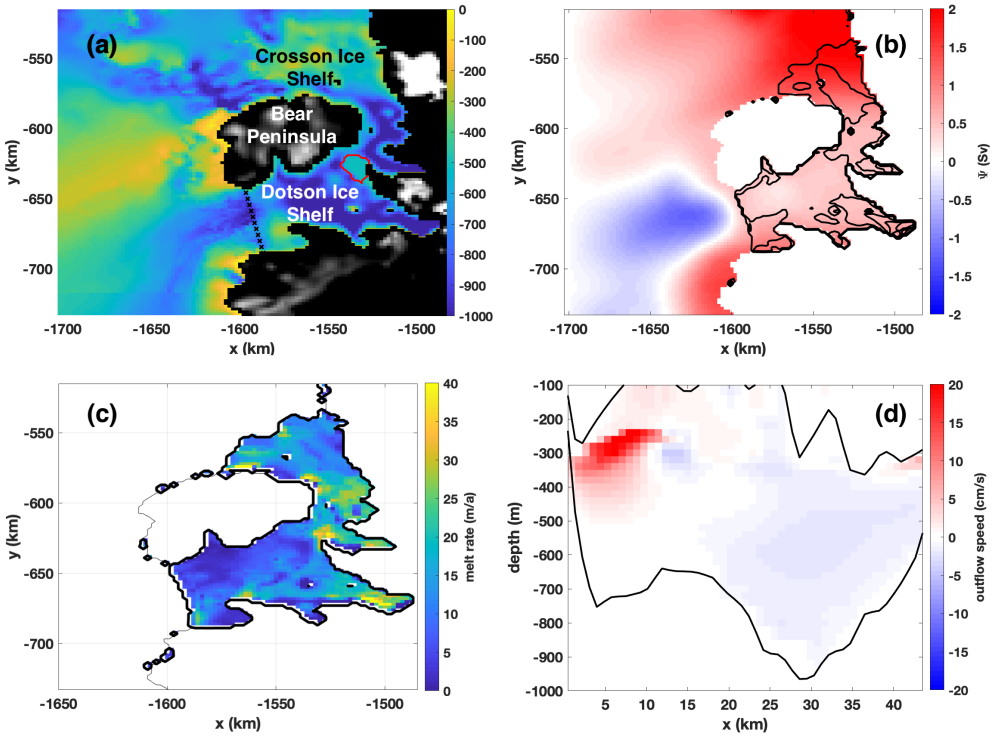

Figure 5. (a) The bathymetry of Millan et al. (2017), used in our adjoint experiment. Black and white shading indicates topography above sea level. X and Y coordinates refer to a Polar Stereographic projection. The cross marks across Dotson ice shelf front indicate the location of the velocity profile in (d), where the bottom edge of the transect corresponds to the left edge of (d). The red contour near the junction of Dotson and Crosson ice shelves indicates where bathymetry has been modified from Millan et al. (2017) as discussed in Section 4.1. (b) The barotropic stream function corresponding to the initial steady state of the ocean model (shading), and ice-shelf topography (contours, 150 m spacing). (c) Under-ice shelf melt rate corresponding to the steady state. (d) Outflow at the opening to the Dotson Ice Shelf cavity cf. Randall-Goodwin et al. (2015), their Figure 7(a)).

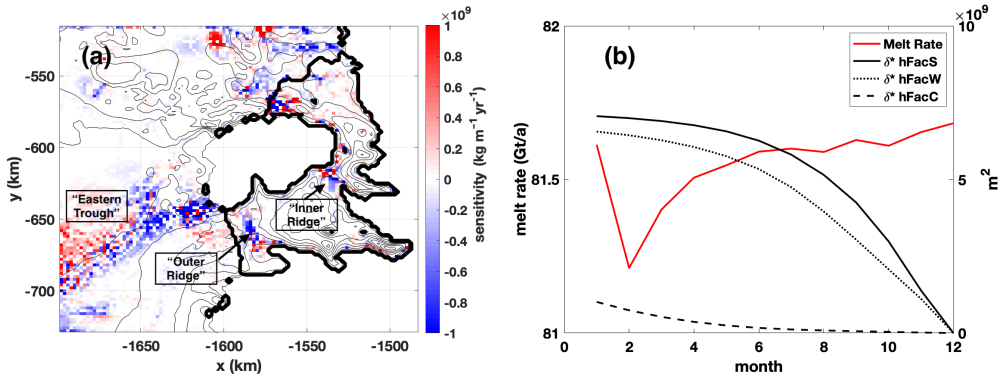

Figure 6. (a) Sensitivity of total (area-integrated) melt to bathymetry in Dotson-Crosson experiment (shading); interpretation is as in Fig. 3(a). Bathymetry is given by thin black contours (200 m spacing) and the boundary of the ice shelf by thick contours. Labels indicate regions discussed in Section 4.2. (b) Time series of melt volume and bathymetric factor sensitivities in our simulation of Dotson and Crosson ice shelves. The bathymetric factors h_f, h_f^s and h_f^w determine the proportion of the bottom cell that is fluid filled, in the center, southern face and western face, respectively. Note sensitivity fields computed from the adjoint model evolve backward in time.

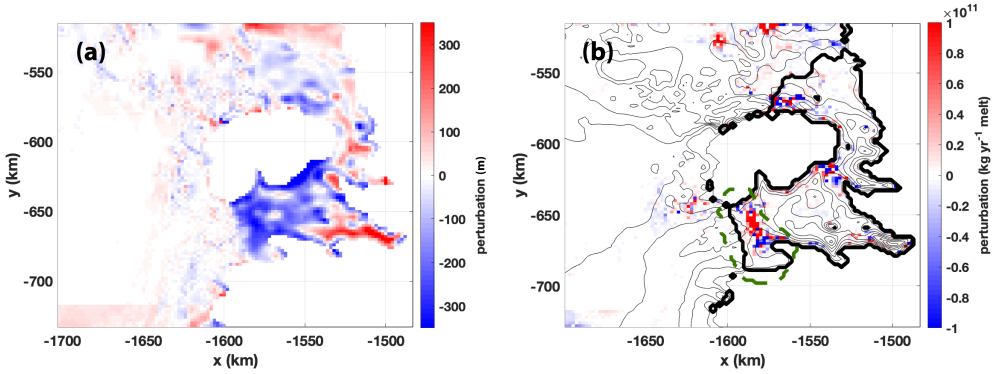

Figure 7. (a) Difference between BedMachine bathymetry and Millan bathymetry within the ocean model domain. The rectangular region in the bottom left of the figure is due to the Millan data set not extending to the edge of the domain. (b) The product of this difference and the sensitivity of melt with respect to bathymetry. The the dashed contour indicates the region in which Millan bathymetry is replaced by BedMachine bathymetry in the perturbation experiment described in Section 4.4.

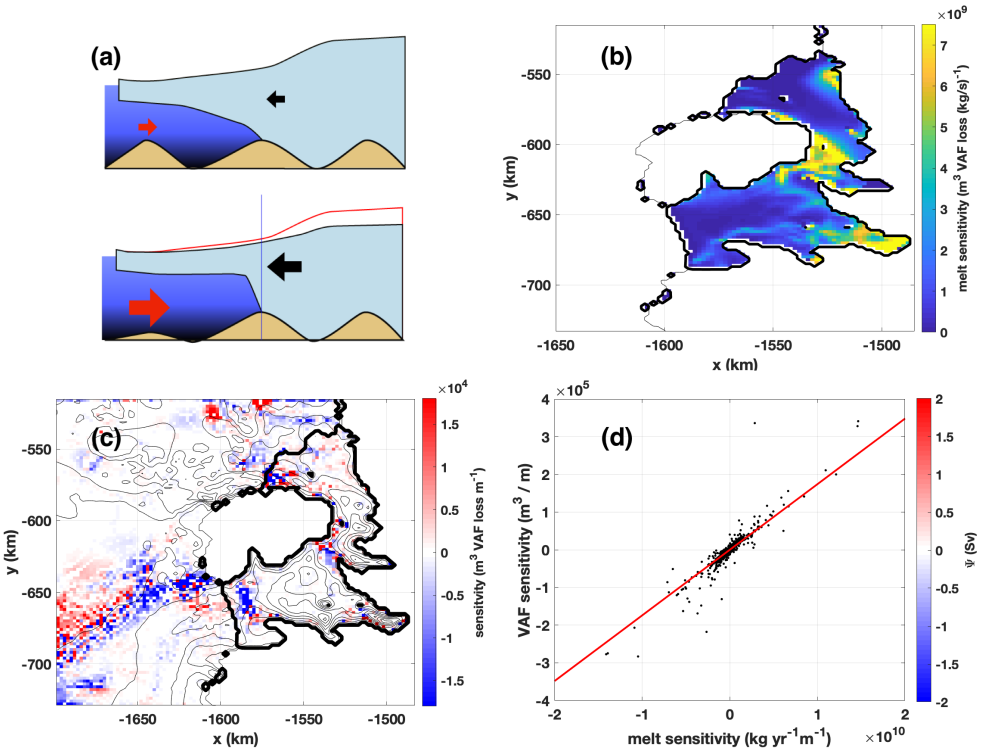

Figure 8. (a) A cartoon illustration of a potential pathyway of influence from bed elevation to grounded ice volume. A lowering of bathymetry in the bottom panel relative to the top allows increased ocean heat flux (red arrows) toward the ice-shelf base, driving melting and thinning. The loss of ice-shelf buttressing causes increased ice volume flux across the grounding line (black arrows), and drawdown of grounded ice. "Grounded ice volume" refers only to the loss of ice upstream of the grounding line, i.e. to the right of the thin vertical blue line; the direct contribution to sea levels from loss of ice-shelf volume is negligible. (b) Sensitivity of grounded ice volume to ice-shelf melt (adapted from Goldberg et al. (2019), their Fig. 3(b)). (c) Sensitivity of the objective function given by Eqn. (6) to bathymetry. (d) Cell-by-cell correspondence of grounded volume sensitivity to melt-rate sensitivity.